Semi-analytical and numerical models to investigate the regulation of shock response spectrum generating in plates

Chengwu Liu*[a], Songwei Cao[b], Feng Xu[a], Yangyu Duan[a], Jingjing Wen[c] and Bin Wu[a]
[a] School of Astronautics, Northwestern Polytechnical University, Xi'an, Shanxi, China; [b] Beijing Shiny Tech. Co., Ltd., Beijing, China; [c] Suzhou Dongling Vibration Test Instrument Co., Ltd., Suzhou, Jiangsu, China

ABSTRACT

In this work, a semi-analytical model of shock response spectrum (SRS) in rectangular plates under impulse loads is carried out. Firstly, the modal analysis technique is employed to solve the acceleration response of rectangular Reissner-Mindlin plates with simply-supported edges. Then, semi-analytical expression of corresponding SRS is obtained after introducing the convolution integrals. With the semi-analytical model, the characteristics of SRS with input variable parameters, such as excitation load and dynamic parameters of plates, are analyzed systematically. Subsequently, a finite element model (FEM) of rectangular Reissner-Mindlin plate is developed to study and verify the regulation effect of excitation load (peak and duration) on the characteristics of SRS. The simulation results indicate that the response accelerations and corresponding SRS of plate agree well with the regulations from semi-analytical model. Lastly, rectangular Reissner-Mindlin plates with various variable parameters are simulated with FEM model to further explore the regulation effects of SRS, and results indicate characteristics of SRS are highly dependent on each input variable (excitation load, dynamic characteristic, response position and boundary condition of plate).

Keywords: Pyroshock test, SRS, Reissner-Mindlin plate, FEM

1. INTRODUCTION

The response of mechanical structure with a shock excitation applied is characterized by transient decaying motions called pyroshock[1]. In aerospace mission, the pyroshock plays an important role in the explosion of ordnance devices during separation of equipment, opening of solar sails or the launch of a satellite, which may cause failures of fragile components and structures, especially in electronic equipment[2-5]. Therefore, it is necessary to perform pyroshock tests for the sensitive elements of a space flight at first in order to evaluate and assure its functionality. Owing to the complexity and uncertainty of pyroshock environment, it is difficult to describe the shock propagation and its level in the structures. Therefore, the concept of shock response spectrum (SRS) is proposed to characterize and simulate the real pyroshock environment in laboratory, and become a widespread tool in pyroshock tests[6]. The SRS is broadly defined as the peak response of an array of n damped single degree of freedom (SDOF) oscillators (mass is m_i, stiffness is k_i and damping is $c_i = 0.1\sqrt{m_i k_i}$) to an excitation as a function of the nature frequency (f_i) of the oscillators and their peak acceleration ($a_i = \max|\ddot{x}_i(t)|$) are mostly used in aerospace engineering (see Figure 1)[7,8]. In order to establish the specification of SRS tests, governments and aerospace administrations define a series of standards, such as MIL, NASA and IEST, that provides strict requirements and techniques for pyroshock tests[9-11].

According to the characteristics of pyroshock signal (high acceleration and bandwidth), the proposed SRS standards describe the pyroshock environment as a polygonal line (corner frequency and peak acceleration plateau) and SRS tolerances. When the pyroshock test generates a specific SRS without leaving the tolerance lines prescribed, it is confirmed that the pyroshock environment is replicated correctly[12,13]. Figure 2 has shown an example of SRS standard with the given tolerances. To fulfill the test standards and make SRS within the well-define tolerance, there are three main types empolyed in pyroshock tests (electrodynamic shaker, mechanical impact and initiating explosive devices). The electrodynamic shaker is used to simulate the pyroshock environment by its feasibility[14], but is rarely adopted in far-field pyroshock tests due to its limitation of peak acceleration and bandwidth. The generation peak acceleration of SRS by electrodynamic shaker can only reach 2000g within a bandwidth of less than 5kHz[15]. The method of mechanical impact-typed test is usually used for

* liu_1992@mail.nwpu.edu.cn, phone:15114041992

International Conference on Optics, Electronics, and Communication Engineering (OECE 2024), edited by Yang Yue, Proc. of SPIE Vol. 13395, 133951X · © 2024 SPIE · 0277-786X · Published under a Creative Commons Attribution CC-BY 3.0 License · doi: 10.1117/12.3049872

mid- and far-field pyroshock environment with peak acceleration varying from 1000-5000g and substantial spectral content above 5000Hz[16]. The resonant facility, such as plates or beams, is struck with an impactor and generates transient acceleration signal, which makes pyroshock tests more convenient[17,18]. The third method for near-field pyroshock test is initiating explosive devices, its peak acceleration could exceed 5000g and frequency above 10kHz[19], but the hazard and low repeatability limit the application of this method[20]. As noted above, the mechanical impact-typed pyroshock test become most commonly applied in aerospace engineering due to its controllability and reproducibility.

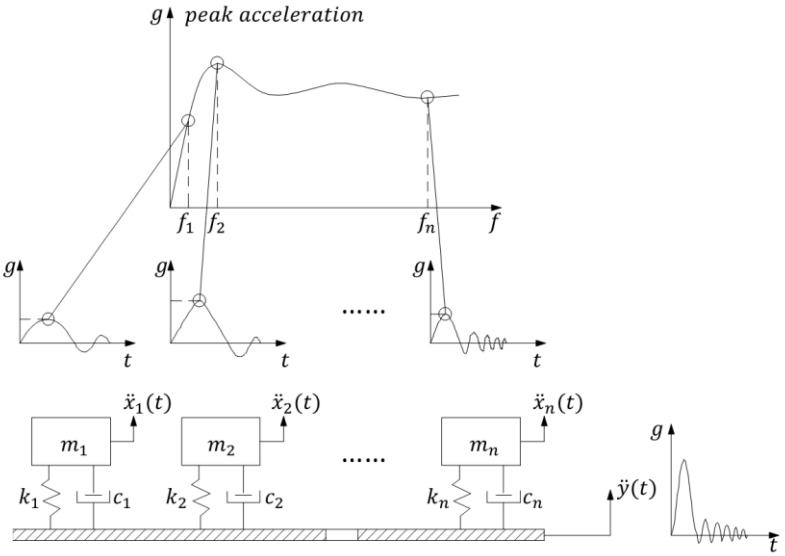

Figure 1. Scheme for SRS concept.

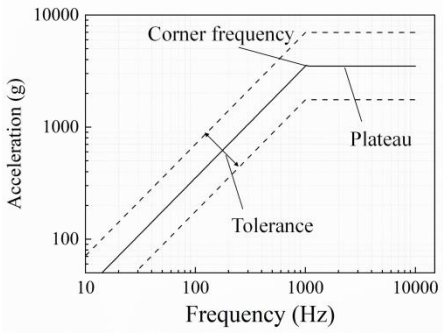

Figure 2. An example of SRS standard.

A main advantage of the mechanical impact-typed pyroshock test lies in the ability to match the desired SRS profile by changing the parameters of the setup (input load or resonant facility). However, obtaining an expected SRS by mechanical impact test is not easy owing to lack the systematic studies on the generating mechanism of resonant facility. Consequently, to acquire desired SRS and simulate pyroshock environment accurately, it is necessary to investigate the relationship between the variable parameters of the setup for pyroshock test (characteristics of the resonant facility, impulse loads, response position or boundary condition) and the corresponding SRS. To this end, R. David et al.[21]proposed the analytical expressions for the various common SRS forms, in which the impulsive mechanical-load was employed as the shock input. This method obtains the analytical SRS forms due to the simplified impulsive input load, which is not coincident with real pyroshock environment. Following with this study, David[22] calculated the shock response of a thin plate with transverse load, and the results were verified by finite element analysis (FEA). Considering that pyroshock signal is simulated by the resonant facility, such as beam and plate, there are many researches focusing on the response of plate or beam. Liew et al.[23] conducted the vibration analysis of Mindlin plates by setting boundary characteristic orthogonal polynomials, and obtained the exact solution of the eigenvalue of thick plate. Reddy et al.[24] studied the relationship for solution of the classical plate theory and its shear deformation, which improved the accuracy of the numerical results. Reynolds et al.[25]

considered the low accuracy at high frequency of the FEA, the asymptotic modal analysis was used for the approximate solutions of the transient response of a panel. However, the relationship between the response of plate and corresponding SRS is insufficient. By combining the response of plate with the characteristic of SRS, Botta et al.[26] evaluated the relationship of characteristic of SRS with geometric parameters of Mindlin plate under various impulsive loads, which presented a link between the resonant plate and corresponding SRS. However, this research focuses on the influence of rise ramp of impulse without experimental verification. Parzianello et al.[27] analyzed the effects of the input parameters of trapezoidal force on the characteristic of SRS, and introduced a method to match an experimental signal using a FEA model with combination of force impulses. Subsequently, Lacher et al.[28] proposed a mechanical model that consisted of the contact between the rigid sphere and a free deformable plate. By studying the theory of impact and propagation of longitudinal stress wave, the model provided a semi-analytical solution of the response of plate. Based on this model, Morais et al[29] provided a comprehensive study and characterization of the pendular resonant shock test system, in which the comparison between the FEA and experiment was carried out. Li et al.[30] additionally considered a slender beam under impulsive load and the yield strength of structure by FEM simulation.

In summary, the previous literatures about the impact-typed SRS are lack of the systematic study for relationship between the shock input, dynamic characteristic of resonant facility and corresponding SRS characteristic. The main deficiencies can be summarized as follow:

(1) The analytical solution for response of resonant facility including experimental verification is neglected. Botta et al.[26] established the analytical model of response of the Mindlin plate and studied the influence of ramp type of impulse on SRSs without corresponding experimental verification. Similarly, Parzianello et al.[27] considered the force input shape effect on SRS curve, and conducted the hypervelocity impact experiment to match the SRS mainly based on FEA and SEA without analytical calculation.

(2) Most of the preceding studies only presented the semi-analytical solutions of SRS by the expressions of the response of resonant facility. David et al.[22] and Lacher et al.[28] obtained the analytical expressions for a rectangular plate under the transverse and longitudinal shock loading respectively without calculating the SRS analytically. Although the R. David et al.[21] provided the analytical descriptions of various SRSs, considering the impulsive loads as the shock inputs $\ddot{y}(t)$ (shown in Figure1), which was not coincident with real pyroshock signals.

(3) There is no practical guidance for engineers to perform pyroshock tests. The preceding literatures[26-29] had investigated the relationship between the impulsive load, response positions and SRSs. However, the methods to match the desired SRS profile were not given, thus, the conclusions of these studies cannot be applied to engineering.

The number of literatures on SRS combining the theoretical with experimental results is quite insufficient, and the analytical calculation of SRS under impulsive load needs to be carried out, to the best of the authors' knowledge. This paper proposes a semi-analytical solution of SRS by Reissner-Mindlin plate theory, modal analysis technique and the convolution integrals. The relationship between dynamic characteristics of the resonant plate, input loads, response position, boundary condition and corresponding SRS characteristic is investigated by a semi-analytical expression of SRS. Meanwhile, a finite element model (FEM) is established and series of simulations are conducted to verify the relationship between the SRS and each experimental variable.

2. REISSNER-MINDLIN PLATE THEORY

The theory of Reissner-Mindlin plates provides reasonably accurate estimation for moderately thick plates[31]. Different from the Kirchhoff-Love model, Mindlin plate model takes into account the shear deformability and rotatory inertia, and natural modes at high frequencies will not be omitted, which is significant as the thickness span increases[32-34]. To accomplish the analytical solutions of SRS, the method of modal superposition is applied to calculate the response of a rectangular plate with four simply-supported edges when an impulsive shock is inputted. And the algebraic expressions of corresponding SRS can be presented by the convolution integrals.

2.1 The eigenfrequencies of simply-supported plate

Consider a flat, isotropic and rectangular plate of uniform thickness (h), length (a), width (b), Young's modulus (E), Poisson's ratio (v) and mass density (ρ). It is simply-supported on all four edges and subjected to a transverse point force P, as shown in Figure 3.

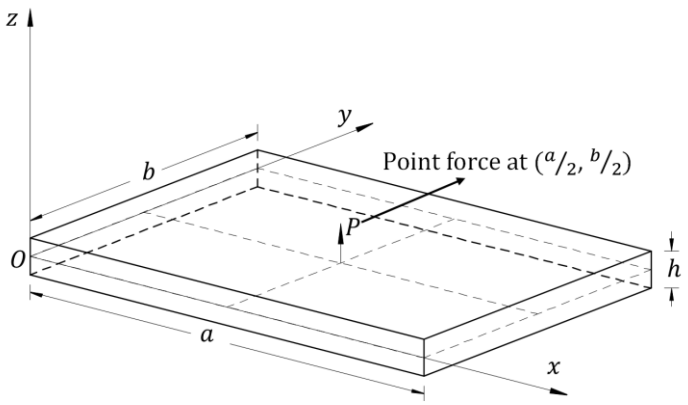

Figure 3. Simply-supported plate reference configuration.

The constitutive equation that governs free vibrations of Reissner-Mindlin plates is well-known[35]. By combining the strain, stress tensor with the equilibrium equations in terms of displacements and loads, the equation for Mindlin plate is obtained:

$$D\nabla^4 w + \omega^2\rho\left(\frac{D}{\eta}+\frac{h^3}{12}\right)\nabla^2 w + \omega^2\left(\frac{h^3\omega^2\rho^2}{12\eta}-\rho h\right)w = 0 \; or \; P \tag{1}$$

Where $D = E\,h^3/[12(1-\nu^2)]$ is the flexural rigidity and $\eta = G\kappa^2$ is the shear coefficient ($G = E/[2(1+\nu)]$ is the shear modulus and $\kappa^2 = 5/6\; or\; \pi^2/12$ is the shear correction factor[36]). w is defined as the transverse (z-direction) displacement of the neutral surface and ∇^4 is the dual application of the Laplacian operator.

The simply-supported boundary conditions can be written as:

$$w = 0 \quad \psi_s = 0 \quad M_n = 0 \tag{2}$$

Where the ψ and M are the bending rotation and moment of edge, their subscript notation s, n denote the normal and tangential directions, respectively. Thus, the analytical transverse eigenmodes are expressed by

$$W_{mn}(x,y) = sin\frac{m\pi x}{a}sin\frac{n\pi y}{b} \tag{3}$$

And the rotation eigenmodes are:

$$\Psi_{mn}(x,y) = -C_{mn}\pi\begin{cases}\frac{m}{a}cos\frac{m\pi x}{a}sin\frac{n\pi y}{b}\\ \frac{n}{b}sin\frac{m\pi x}{a}cos\frac{n\pi y}{b}\end{cases} \tag{4}$$

The coefficients of rotation eigenmodes are:

$$C_{mn} = \frac{(\frac{m\pi}{a})^2+(\frac{n\pi}{b})^2-\frac{\rho\omega_{mn}^2}{\eta}}{(\frac{m\pi}{a})^2+(\frac{n\pi}{b})^2} = 1-\frac{1}{\eta}\sqrt{\frac{\rho D}{h}}\frac{\omega_{mn}^2}{\widehat{\omega}_{mn}^{KL}} \tag{5}$$

With the frequency of vibration of the Kirchhoff-Love plate[37]

$$\widehat{\omega}_{mn}^{KL} = \pi^2(\sqrt{\frac{D}{\rho h}})(\frac{m^2}{a^2}+\frac{n^2}{b^2}) \tag{6}$$

Substituting the Eq. (3) and (4) into Eq. (1), the expression for the natural frequency of simply-supported plate is shown in Eq. (7) below[26]:

$$\omega_{mn}^2 = \frac{1}{2h^3\rho}\left[\sqrt{\frac{\rho h}{D}}\,\widehat{\omega}_{mn}^{KL}h^3\eta + 12\eta h + 12D - \sqrt{(12\eta h + (\eta h^3 + 12D)\sqrt{\frac{\rho h}{D}}\,\widehat{\omega}_{mn}^{KL})^2 - 48h^4\eta\rho(\widehat{\omega}_{mn}^{KL})^2}\right] \tag{7}$$

2.2 The general response of Mindlin plate

As presented in Introduction, the modal analysis technique must be used to calculate the analytical response of Mindlin plate. Consider the undamped plate using the method of modal superposition, the equilibrium equations with the load F can be written as[26]:

$$H\ddot{u} + Lu = F \tag{8}$$

With

$$H = \begin{bmatrix} \rho h^3/12 & 0 & 0 \\ 0 & \rho h^3/12 & 0 \\ 0 & 0 & \rho h \end{bmatrix} \quad u = \begin{bmatrix} \psi_x(x,y,t) \\ \psi_y(x,y,t) \\ w(x,y,t) \end{bmatrix} \quad F = \begin{bmatrix} f_x \\ f_y \\ f_z \end{bmatrix}$$

$$L = \begin{bmatrix} -\frac{D}{2}\left[2\frac{\partial^2}{\partial x^2} + (1-\nu)\frac{\partial^2}{\partial y^2}\right] + h\eta & -\frac{D}{2}(1+\nu)\frac{\partial^2}{\partial x\partial y} & h\eta\frac{\partial}{\partial x} \\ -\frac{D}{2}(1+\nu)\frac{\partial^2}{\partial x\partial y} & -\frac{D}{2}\left[2\frac{\partial^2}{\partial y^2} + (1-\nu)\frac{\partial^2}{\partial x^2}\right] + h\eta & h\eta\frac{\partial}{\partial y} \\ -h\eta\frac{\partial}{\partial x} & -h\eta\frac{\partial}{\partial y} & -h\eta\left(\frac{\partial^2}{\partial x^2} + \frac{\partial^2}{\partial y^2}\right) \end{bmatrix} \tag{9}$$

Where H and L are the mass matrix and stiffness matrix respectively, F is the excited load and u is the response of the plate in each of the coordinate directions.

Therefore, the displacement vector u can be expressed by superposition of corresponding normal modal coordinate $\beta_{mn}(t)$[38]:

$$u(x,y,t) = \sum_{m=1}^{\infty}\sum_{n=1}^{\infty}\beta_{mn}(t)U_{mn}(x,y) = \sum_{m=1}^{\infty}\sum_{n=1}^{\infty}\beta_{mn}(t)\begin{Bmatrix} -\frac{C_{mn}\pi m}{a}\cos\left(\frac{m\pi x}{a}\right)\sin\left(\frac{n\pi y}{b}\right) \\ -\frac{C_{mn}\pi n}{b}\sin\left(\frac{m\pi x}{a}\right)\cos\left(\frac{n\pi y}{b}\right) \\ \sin\left(\frac{m\pi x}{a}\right)\sin\left(\frac{n\pi y}{b}\right) \end{Bmatrix} \tag{10}$$

Substituting Eq. (10) in Eq. (8), the equilibrium equation becomes:

$$\ddot{\beta}_{mn}(t) + \omega_{mn}^2\beta_{mn}(t) = \frac{f_{mn}(t)}{M_{mn}} \tag{11}$$

The generalized mass M_{mn} and load $f_{mn}(t)$ can be obtained by modal orthogonality[39] as below:

$$M_{mn} = \int_0^a\int_0^b U_{mn}^T H U_{mn}\,dxdy = \left(\frac{ab}{4}\right)\left[\rho h + \left(\frac{\pi^2m^2C_{mn}^2}{a^2} + \frac{\pi^2n^2C_{mn}^2}{b^2}\right)\frac{\rho h^3}{12}\right]$$
$$f_{mn}(t) = \int_0^a\int_0^b F U_{mn}\,dxdy \tag{12}$$

And convolution integrals[40] can help to solve Eq. (11):

$$\beta_{mn}(t) = \beta_{mn}(0)\, cos(\omega_{mn}t) + \frac{\dot{\beta}_{mn}(0)}{\omega_{mn}} sin(\omega_{mn}t) + \frac{1}{M_{mn}\omega_{mn}} \int_0^t f_{mn}(\tau)\, sin\, \omega_{mn}(t-\tau)\, d\tau \tag{13}$$

Together with initial conditions:

$$\begin{aligned} \beta_{mn}(0) &= \int_0^a \int_0^b u(x,y,0)\, U_{mn} dxdy \\ \dot{\beta}_{mn}(0) &= \int_0^a \int_0^b \dot{u}(x,y,0)\, U_{mn} dxdy \end{aligned} \tag{14}$$

As for load F, the excitation applied to a resonant facility (beam or plate) is due to the transverse mechanical impact generally. Impact is defined as a sudden contact of a moving body with another one and is a complex phenomenon[41]. There are several contact concepts usually adopted in impact engineering. Newton's law of impact is based on the coefficient of restitution (experiment obtained) to describe two stages of impact (squeeze and restitution)[42]. Hertzian contact theory considers indentation between the rigid sphere and the deformable body and shows the linear elastic properties[43]. Therefore, the contact load can be approximated as a half sine impact according to these concepts. An idealized half-sine impulsive load P at point $(a/2\,, b/2)$ (see in Figure 3) is employed as shock input in this paper, shown in Figure 4.

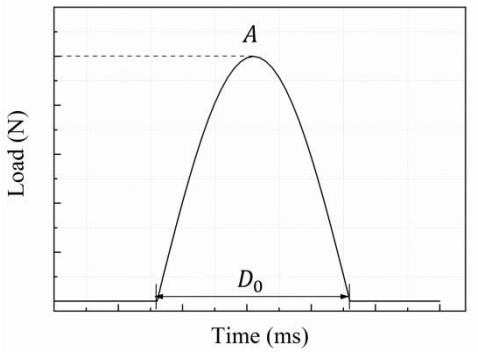

Figure 4. Idealized half-sine impulsive load, where A and D_0 represent the peak and the pulse duration of the shock input respectively.

The transverse point load P is on the centroid $(a/2\,, b/2)$ of neutral plane, thus the excited load F can be expressed by

$$F = \begin{bmatrix} 0 \\ 0 \\ P = A\, sin\, \dfrac{\pi t}{D_0} \end{bmatrix} \tag{15}$$

Introducing the position function $r\,(x,y)$ of transverse point load:

$$r(x,y) = \begin{cases} 1, & (x = a/2\,, y = b/2) \\ 0 \end{cases} \tag{16}$$

And the generalized transverse load $f_{mn}(t)$ will be constructed as:

$$f_{mn}(t) = \int_0^a \int_0^b r(x,y)\, A\, sin\, \frac{\pi t}{D_0} sin\, \frac{m\pi x}{a} sin\, \frac{n\pi y}{b} dxdy = A\, sin\, \frac{\pi t}{D_0} sin\, \frac{m\pi}{2} sin\, \frac{n\pi}{2} \tag{17}$$

Combining the Eq. (10), (11) with Eq. (17), the transverse acceleration response of Mindlin plate on the centroid $(a/2\,, b/2)$ of neutral plane can be obtained:

$$\ddot{w}\left(\frac{a}{2}, \frac{b}{2}, t\right) = \begin{cases} \sum_{m=1}^{\infty} \sum_{n=1}^{\infty} - \dfrac{AD_0\left[\pi\omega_{mn}^2\, sin(\omega_{mn}t) - \frac{1}{D_0}\pi^2\omega_{mn}\, sin\frac{\pi t}{D_0}\right]W^2}{M_{mn}\omega_{mn}(\pi^2 - D_0^2\omega_{mn}^2)}, t \in [0, D_0] \\ \sum_{m=1}^{\infty} \sum_{n=1}^{\infty} - \dfrac{AD_0\pi\left[\omega_{mn}^2\, sin(\omega_{mn}t) - \omega_{mn}^2\, sin\, \omega_{mn}(D_0 - t)\right]W^2}{M_{mn}\omega_{mn}(\pi^2 - D_0^2\omega_{mn}^2)}, t \in [D_0, \infty] \end{cases} \tag{18}$$

Where the analytical expression of acceleration response is composed of the forced vibration $t \in [0, D_0]$ and free vibration $t \in [D_0, \infty]$ of Mindlin plate.

2.3 The semi-analytical solutions of SRS

According to the definition of SRS, the transverse acceleration response of plate Eq. (18) is employed as the shock inputs $\ddot{y}(t)$ of the base in Figure 1, and the maximum absolute acceleration responses of a series of SDOF oscillators to that excitation are solved as the function of the nature frequency of these oscillators. There are several algorithms of the response of the SDOF oscillators to shock input applied in solution of SRS. Convolution integrals originate from superposition of impulse response function in time domain[44]. Fourier transform method is derived by impulse response function, which transforms the integral in time domain into multiplication in frequency domain. Digital filtering method[45] is based on the Z-transform of transfer function, and is most commonly used in engineering due to its high accuracy. In order to analytically accomplish expression of SRS, the non-numerical convolution integral is required. Simplified calculation of the displacement responses of the SDOF oscillators $\ddot{x}_i(t)$ by neglecting their dampers, the convolution integral is written as:

$$\ddot{x}_i(t) = -\frac{1}{\omega_i}\int_0^t \ddot{w}\left(\frac{a}{2}, \frac{b}{2}, \tau\right) sin\, \omega_i(t-\tau)\, d\tau \tag{19}$$

Where $\omega_i = 2\pi f_i$ is the nature cyclic frequency of the oscillator.

Therefore, the analytical response of SDOF oscillator can be expressed by:

$$\ddot{x}_i(t) = \begin{cases} \sum_{m=1}^{\infty}\sum_{n=1}^{\infty} -\dfrac{AD_0\left[\begin{array}{c}\frac{\pi\omega_{mn}^2}{\omega_i^2-\omega_{mn}^2}[\omega_i\, sin(\omega_{mn}t)-\omega_{mn}\, sin(\omega_i t)] \\ -\frac{\pi^3\omega_{mn}\, sin(\omega_i t)-\pi^2\omega_{mn}\omega_i D_0\, sin(\frac{\pi t}{D_0})}{(\pi^2-D_0^2\omega_i^2)}\end{array}\right]W^2}{M_{mn}\omega_i\omega_{mn}(\pi^2-D_0^2\omega_{mn}^2)}, t \in [0, D_0] \\ \sum_{m=1}^{\infty}\sum_{n=1}^{\infty} -\dfrac{AD_0\pi\left[\begin{array}{c}\frac{\omega_{mn}^2}{\omega_i^2-\omega_{mn}^2}[\omega_i\, sin(\omega_{mn}t)-\omega_{mn}\, sin(\omega_i t)] \\ \omega_{mn}^2[\omega_i\, sin\,\omega_{mn}(D_0-t)- \\ -\frac{sin(\omega_{mn}D_0)\, cos(\omega_i t)+\omega_{mn}\, cos(\omega_{mn}D_0)\, sin(\omega_i t)]}{(\omega_i^2-\omega_{mn}^2)}\end{array}\right]W^2}{M_{mn}\omega_i\omega_{mn}(\pi^2-D_0^2\omega_{mn}^2)}, t \in [D_0, \infty] \end{cases} \tag{20}$$

The maximum of Eq. (20) is the peak acceleration of SDOF oscillator and the value of SRS curve. However, the complicated trigonometric functions in Eq. (20) lead to the difficulty in obtaining the analytical expression of SRS, thus, a simplified method need to be employed. Considering the characteristics of trigonometric functions, ± 1 are utilized to replace the $\pm \sin t$ or $\pm \cos t$ in Eq. (20). After combining the responses of forced vibration and free vibration, the semi-analytical model of SRS is obtained as

$$Acc(\omega_i) = max|\ddot{x}_i(t)| \approx \frac{AD_0\pi[2\omega_{mn}^2\omega_i + 2\omega_{mn}^3 + \omega_{mn}^2)]}{M_{mn}\omega_i\omega_{mn}(\pi^2 - D_0^2\omega_{mn}^2)(\omega_i^2 - \omega_{mn}^2)}W^2 \tag{21}$$

There is obvious deviation on the amplitude of SRS in Eq. (21) due to the ignoring of damper and simplification of trigonometric functions. Although, the approximate expression of SRS can be used to analysis the relationship between dynamic characteristics of the resonant facility, impulse transverse loads, response position and corresponding SRS, as follow:

(1) The one part of the denominator $(\omega_i^2 - \omega_{mn}^2)$, where the ω_i and ω_{mn} are the nature cyclic frequency of the SDOF oscillator and Mindlin plate respectively, illustrates that the local peak responses of SRS occur at the partial frequencies of resonant facility (in other words, the convexity of SRS curve will generate when ω_i is equal to ω_{mn}). And the phenomenon of shock spectrum dip effect[46] can form at other nature frequencies of the SDOF oscillator.

(2) The other part of denominator in Eq. (21) $(\pi^2 - D_0^2\omega_{mn}^2)$ can be used to explain the relationship between the impulsive load (P) and the characteristics of SRS. The value of π/D_0 is equivalent to the natural cyclic frequency of the harmonic signal, where the natural half-period is D_0. This indicates that one natural frequency of resonant facility $(\omega_{mn} = \pi/D_0)$ will be excited and local peak of SRS can be excited by impulsive load.

(3) The transverse natural modal (W) of Mindlin plate in Eq. (21) contains the implication that the effect of response position is important for the profile of SRS. The response position of analytical SRS equation derived previously is $(a/2\,,b/2)$, where the expression of W is $\sin m\pi/2 \cdot \sin n\pi/2$. However, the value of second order natural modal ($m = 2\ or\ 1, n = 1\ or\ 2$) is equal to zero at the center point, which is another reason of spectrum dip effect. In fact, as the response position shifts to $(a/4\,,b/4)$, the other natural modal ($m\ or\ n = 4$) can tend to be zero again and corresponding profile of SRS will be changed at different response positions.

3. VERIFICATION WITH SIMULATION

3.1 Finite element model

A finite model of rectangle plate subjected to impulse load is simulated with a commercial finite element software, ABAQUS, to investigate the SRS regulations. The geometry of the 3D FEM employed in this study is shown in Figure 5. Three different plates (1~3) are selected and the corresponding geometrical parameters are set as $400 \times 400 \times 30$mm, $400 \times 400 \times 20$mm and $300 \times 300 \times 30$mm, respectively. The material of these plates is aluminum and values of material properties are listed in Table 1. The boundary condition of the model is defined as simply-supported on all four edges, as shown in Figure 5. To be consistent with the semi-analytical model, the half-sine impulsive load is applied in the center position of the plate. For the mesh, the structured technique and medial axis algorithm were used to realize the hexahedral element shape. Generally, C3D8R elements are applied for modal-superposition response analysis. After the basic setup of the FEM, the time of calculation is about 15ms to guarantee adequate response duration, and three response positions (1~3) are extracted to analyze.

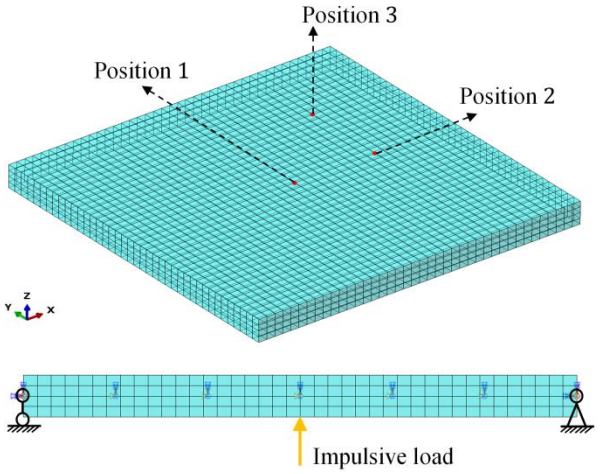

Figure 5. Schematic of 3D FEM.

Table 1. Values of material parameters of aluminum.

Materials	Density (kg/m^3)	Young's modulus (MPa)	Poisson's ration
Aluminum	2700	71000	0.3

Considering the sufficient mesh density is crucial for the validity of the simulation, the mesh-independent convergence of the simulation model should be assessed at first. Therefore, five mesh sizes ranging from 6 to 14mm are determined for plate-1. The peak and duration of impulsive load are defined as 10000N and 1ms, and the response acceleration in the position 1 is selected to estimated. The results of the mesh-independent convergence are shown in Figure 6. There are obvious deviations on response acceleration curves when the mesh size is set as 12mm and 4mm, but the response acceleration converged to the certain trend for mesh size below 10mm. Considering that the height of the plate was 30mm, the number of meshes was sufficient to obtain convergence trend. Thus, the critical mesh size was set to 10mm, and the total numbers of elements and nodes for the FEM are 6400 and 31549, respectively.

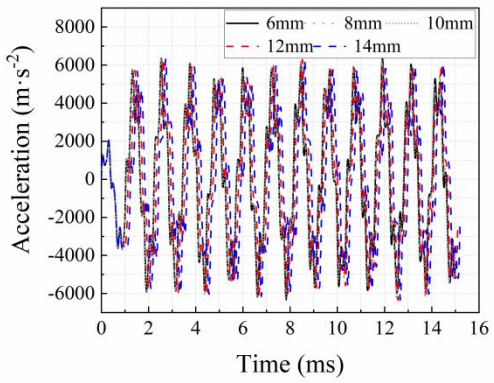

Figure 6. Mesh-independent convergence evaluation.

3.2 Comparison between semi-analytical model and FEM

To evaluate the effectivity of the FEM, three impulsive loads with different input parameters are applied in plate-1, and the response accelerations in position-1 from semi-analytical and FEM are selected to compare, in which the modal parameter (natural frequency), response acceleration and corresponding SRSs from semi-analytical and FEM are shown in Table 2 and Figure 7 (a-c). It can be found the simulated results are almost in agreement with the theoretical results, except for the tiny deviation of each order natural frequencies which may originate from the degree of mesh dispersion of simulation model. The maximum relative error of natural frequency between analytical expression in Eq. (7) and simulation is about 3%. As for response acceleration and SRSs, low-frequency components show a certain deviation and the errors become more obvious due to the double logarithmic coordinates of figures. The overall responses from simulation model agree well with semi-analytical model, which indicates developed FEM is suitable for describing the shock response of plate.

Table 2. Natural frequency comparisons between the analytical expression and simulation.

Results	Order of natural frequency (Hz)					
	1	2	3	4	5	6
Analytical expression	885.6	2150.1	3353.7	4125.3	5241.3	6660.5
Simulation	870.8	2114.6	3252.3	4096.8	5097.1	6649.4
Relative error (%)	1.69	1.67	3.01	0.71	2.75	0.17

Among the results, the partial peaks of SRSs appeared at some certain natural frequencies of the simply-support plate, these frequencies are mainly the first, fourth and sixth order modal of plate-1, which verifies the relationship between the dynamic characteristics of resonant plate and SRS profile preliminarily. Comparing the SRSs in Figure 7 (a) and (c), the maximum of SRSs changes with different peak of impulsive loads, it is obvious that the overall profile of SRSs does not change with the same duration of shock load. Interestingly, the peak value of SRS decreases with increasing input durations in Figure 7 (a) and (b). Therefore, it can be deduced that the coupling effect of the peak responses and input durations need to be considered in SRS experiments. In summary, the results from simulation agree well with semi-analytical model and the partial SRS regulations obtained from semi-analytical model prove to be valid.

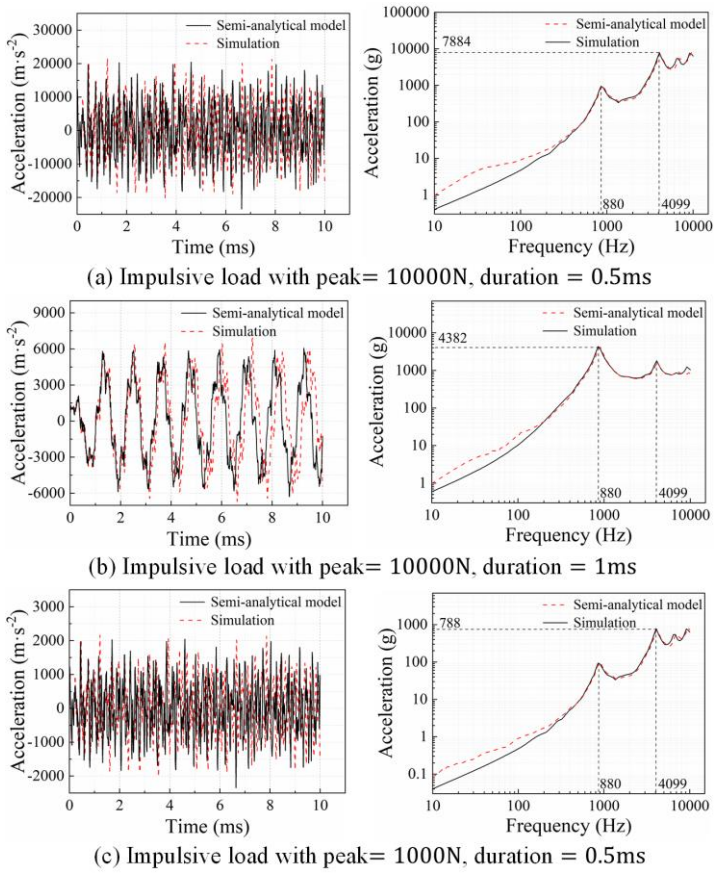

Figure 7. Comparisons of response acceleration and SRSs between semi-analytical expression and simulation.

4. SRS REGULATION DISCUSSION

With the aim to further systematical verification of SRS regulation effects, a series of simulation experiments are performed for parameterized analysis. The characteristics of SRS will be discussed by employing the five variables: peak of impulsive load, duration of impulsive load, natural frequency of resonant plate, response position of plate and boundary condition of plates. The natural frequency can be varied by using plates with different geometrical parameters as aforementioned in subsection 3.1. Three boundary conditions are applied on the edges of plates, where S represents simple-support, F means free and C is clamped. The sample groups of simulation are summarized in Table 3.

Table 3. Parameterized analysis of SRS regulation.

Sequence of groups	Variable				
	Peak of load (N)	Duration of load (ms)	Sequence of plates	Sequence response position	Boundary condition
Group 1	10000	0.5	Plate-1	Position-1	SSSS
Group 2	10000	1	Plate-1	Position-1	SSSS
Group 3	10000	2	Plate-1	Position-1	SSSS
Group 4	10000	10	Plate-1	Position-1	SSSS
Group 5	5000	1	Plate-1	Position-1	SSSS
Group 6	15000	1	Plate-1	Position-1	SSSS
Group 7	20000	1	Plate-1	Position-1	SSSS
Group 8	10000	1	Plate-2	Position-1	SSSS
Group 9	10000	1	Plate-3	Position-1	SSSS
Group 10	10000	1	Plate-1	Position-2	SSSS

Sequence of groups	Variable				
	Peak of load (N)	Duration of load (ms)	Sequence of plates	Sequence response position	Boundary condition
Group 11	10000	1	Plate-1	Position-3	SSSS
Group 12	10000	1	Plate-1	Position-1	CCFF
Group 13	10000	1	Plate-1	Position-1	CCCC

4.1 Effect of impulsive load

In order to study the effect of impulsive load on the SRS, the simulation results of groups 1~7 are presented in Figure 8 and Figure 9. From Figure 8, it can be observed that both maximum of response acceleration and SRS decrease as the increasing duration of load. This can be attributed to the concentrated low frequency energy for large duration of impulsive loads. Therefore, the high frequency response of plate is not excited, which causes lower peak acceleration. In addition, both first and fourth order natural frequencies are excited with different duration, which indicates that the sensitivity of the first and fourth order modal of plate is higher than the rest modal. Furthermore, as the duration of load increases to 10ms, the low frequency response of SRS in group 4 becomes strong, as shown in Figure 8 (b), and the location of low frequency (100Hz) corresponds exactly to the frequency according to the duration of load. This is consistent with the regulation aforementioned in section 2. Figure 9 shows the peak of load effect on the response acceleration and corresponding SRS. The obvious regulation can be found that the overall responses of SRSs elevate as the peak load increases. Owing to the peak of impulsive load has little effect on frequency range of excitation energy, the profile of SRS is not sensitive to the peak of loads. Similarly, the partial natural frequencies of plate can also be observed in Figure 9 (b).

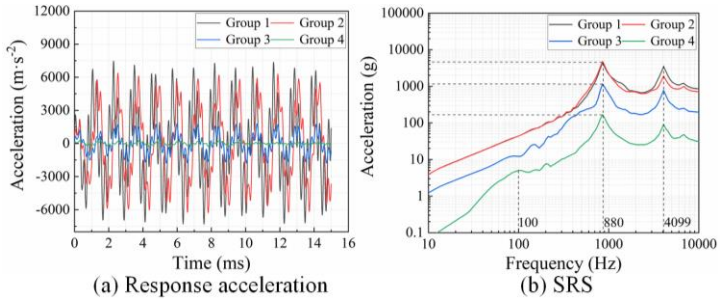

Figure 8. Duration effect on response acceleration and SRS.

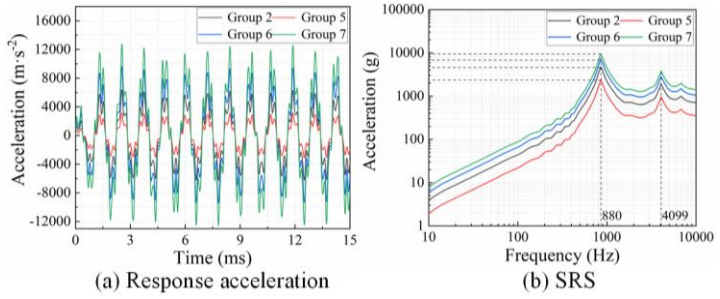

Figure 9. Peak effect on response acceleration and SRS.

4.2 Effect of natural frequency

Figure 10 compares the response acceleration and characteristics of SRS with three different plates. Owing to different geometrical parameters, the natural frequencies are different. After simulating with FEM, the first order natural frequency of plate-2 and -3 are 583Hz and 1559Hz, respectively. With the same boundary condition, the stiffness of thicker plate becomes larger, leading to higher natural frequencies, but the stiffness decreases as the edge length of plate increase. Therefore, the corner frequency of SRS in plate will change when the dynamic characteristic of plates become different. Another interesting phenomenon is that the response accelerations and peak of SRS are also related to natural frequency of plate. As the natural frequency of plate increases, the peak of response decreases obviously. It can be deduced that high

frequency vibration predominates in the response of structures with higher stiffness, these structures can only be excited in larger amplitude under shock input with higher energy. Thus, the response acceleration of plate-3 is the least compared with other plates, as shown in Figure 10 (a). What's more, there are some local peak accelerations in the SRSs within high frequency range, which represents the higher natural frequencies of plates.

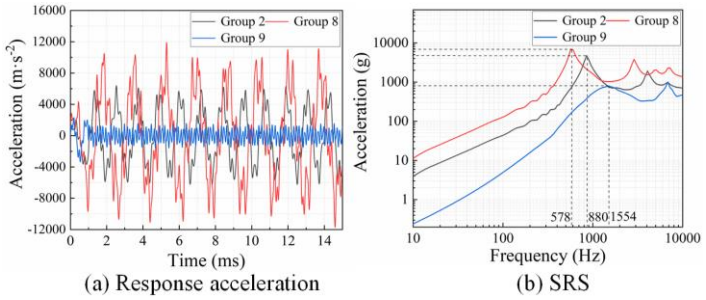

Figure 10. Natural frequency effect on response acceleration and SRS.

4.3 Effect of response position

To determine the effect of response position in SRS, the response accelerations in three different positions are collected and displayed in Figure 11. The maximum of response acceleration decreases as the distance between excited point and acquisition position increases. This may be attributed to the energy losses during the in-plate propagation of vibration. Meanwhile, the peak acceleration of SRS exhibits similar trend, as shown in Figure 11 (b). It is important to note that the local peak responses of SRSs within high frequency range is different at various positions. The first order natural frequency of plate still dominates the vibration of plates in different positions. However, the second order natural frequency is excited in the position-2, and fourth order frequency disappears at this point. To further explore the relationship between local peak in SRS and positions, the partial modal of plate-1 are presented in Figure 12. It can be found that the first and sixth modal can be excited in all positions, but the second modal in position-1 will not be present during the vibration. Similarly, the fourth modal in in position-2 are not obvious. Therefore, there is a small local peak in SRSs of group 10 and 11, but it is smooth at 4099Hz in the SRS of group 10. It can be concluded that the local peak response in SRS is mainly dependent on the position of acquisition.

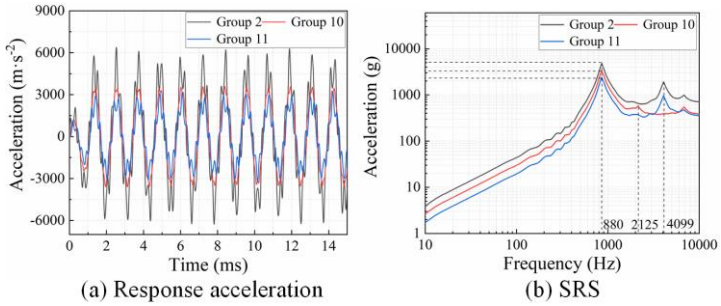

Figure 11. Response position effect on response acceleration and SRS.

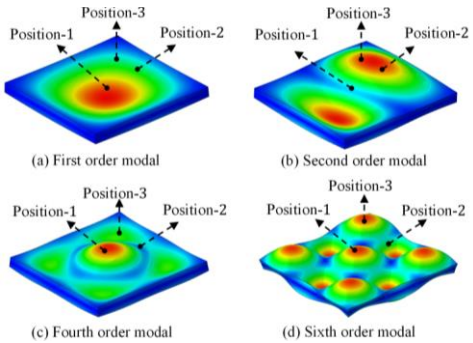

Figure 12. Partial modal of plate-1.

4.4 Effect of boundary condition

In order to investigate the effect of boundary condition on the characteristics of SRS, two different boundary conditions are applied in the plate-1, respectively. Similarly, the response acceleration of plate with four edges clamped exhibits highest first order natural frequency but lowest amplitude, as shown in Figure 13. The first of natural frequency of plate with two edges free and other two edges clamped is about 314Hz, thus, the local peak at SRS of group 12 exists at that frequency. However, the conner frequency is not the first natural frequency in group 12, and the frequency of peak acceleration corresponds to 1164Hz, which is the second natural frequency of plate. Furthermore, the duration of load is 1ms, and the corresponding frequency is about 1000Hz. Therefore, it can be deduced that the conner frequency also depends on the frequency corresponding to the duration of excitation load to some extent. In fact, the changes of boundary condition of plate mean the variation of its natural frequency, thus, the regulation of SRS can also be explained with previous conclusions.

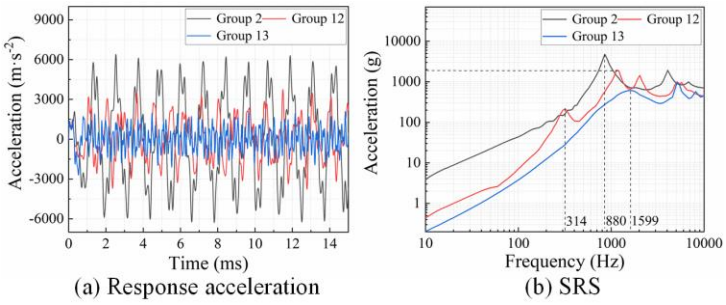

Figure 13. Boundary condition effect on response acceleration and SRS.

5. CONCLUSIONS

In this paper, the semi-analytical expression of SRS is obtained by combining with the Mindlin plate theory, modal analysis technique and the convolution integrals. The relationship between the resonant plate, impulse loads, response position and corresponding SRS are summarized according to the semi-analytical model. Meanwhile, the simulation model is developed and verified to be valid.

The semi-analytical model of SRS and corresponding simulation results show that: (1) The dynamic characteristics of resonant plate, especially the natural frequency, determine the profile of SRS and the local peaks of SRSs which correspond to partial natural frequencies, (2) The peak and duration of impulsive load have large influence on the response acceleration level of SRS. The profile of SRS shows increasing trend with the increasing peak of load but decreasing trend with the increasing duration. Meanwhile the duration of load affects the corner frequency of SRS to some extent when the duration of load equals to the nature half-period of plate resonant facility, (3) The different natural frequencies will be presented at different response positions, and the local peaks of SRS will be displayed at different response points, (4) the boundary condition of plate can change the dynamic characteristics of plate, leading to different profiles of SRSs.

The works in this paper are conducive to accurately analyze the effect of variable parameters on the characteristics of SRS, which is beneficial to efficiently design the resonant facility, shock input and response position to satisfy the pyroshock test requirement. Additionally, this research also offers the adjustment guidance for engineers, which is instructive to improve the efficiency of pyroshock experiments.

REFERENCES

[1] Hwang, J. H, J. and Duran, A., “Stochastic shock response spectrum decomposition method based on probabilistic definitions of temporal peak acceleration, spectral energy, and phase lag distributions of mechanical impact pyrotechnic shock test data,” Mechanical Systems and Signal Processing, 76, 424-440 (2016).

[2] Vijayan, K., and Woodhouse, J, “Shock amplification, curve veering and the role of damping,” Journal of Sound and Vibration, 333(5), 1379-1389 (2014).

[3] Wen, J., Liu, C., Yao, H. and Wu, B., " A nonlinear dynamic model and parameters identification method for predicting the shock pulse of rubber waveform generator," International Journal of Impact Engineering, 120, 1-15 (2018).
[4] Lee, D, O., Han, J, H., Jang, H, W., Woo, S, H., and Kim, K, W., "Shock response prediction of a low altitude earth observation satellite during launch vehicle separation," International Journal of Aeronautical and Space Sciences, 11(1), 49-57 (2010).
[5] Shi, Q., Ando, S., Seko, H., Nagahama, K., and Saegusa, H., "The summarization of pyro-shock testing data and srs level prediction methodology," In Environmental Testing for Space Programmes , 558, 549-554, (2004).
[6] Ho, J. and Hwang, J., "Shock Response Spectrum Decomposition Method Based on Estimation Maximum Input Acceleration and Equivalent Spectral Energy," In 13th European Conference on Spacecraft Structures, Materials & Environmental Testing,727, 97 (2014).
[7] Brake, M, R., "An inverse shock response spectrum," Mechanical Systems and Signal Processing, 25(7), 2654-2672 (2011).
[8] Wijker, J, J., Spacecraft Structures. Springer Science & Business Media, Berlin, 1-5 (2008).
[9] Caruso, H., "MIL-STD-810F, test method standard for environmental engineering considerations and laboratory tests," Journal of the IEST, 44(3), 30 (2001).
[10] Kern, D, L., Status of a NASA Standard and Three NASA Handbooks, USA, (2011).
[11] Walter, P, L., "Accelerometer limitations for pyroshock measurements," Sound and Vibration, 43(6), 17 (2009).
[12] Alexander, J, E., Shock response spectrum-a primer. Sound & vibration, 43(6), 6-15, (2009).
[13] Lalanne, C., "Mechanical vibration and shock analysis, fatigue damage," John Wiley & Sons, 4, 1-2 (2014)
[14] Smallwood, D, O., "Pyroshock testing—electrodynamic shakers," The Journal of the Acoustical Society of America, 111(5), 2381-2381 (2002)..
[15] Davie, N., "Simulation of pyroshock environments using a tunable resonant fixture," U.S. Department of Energy Office of Scientific and Technical Information - OSTI OAI,U.S. Department of Energy Office of Scientific and Technical Information - OSTI OAI (1996).
[16] Morais, O, M, F., Vasques, C, M, A., Perestrelo, C., Pimenta, V. and Baldesi, G., "Functional verification and performance tests of an ultra-low shock non-explosive actuator for hold-down and release mechanisms for space applications," Proceedings of the Institution of Mechanical Engineers, Part G: Journal of Aerospace Engineering 228(13), 2487-2495 (2014).
[17] Gherlone, M., Lomario, D., Mattone, M. and Ruotolo, R., "Application of wave propagation to pyroshock analysis," Shock and Vibration, 11(3-4), 145-156 (2004).
[18] Hu, B., Schiehlen, W. and Eberhard, P., "Comparison of analytical and experimental results for longitudinal impacts on elastic rods," Journal of Vibration and Control, 9(1-2), 157-174 (2003).
[19] D. Wattiaux, O. Verlinden, C. Conti, and C. De Fruytier, "Prediction of the Vibration Levels Generated by Pyrotechnic Shocks Using an Approach by Equivalent Mechanical Shock," Journal of Vibration and Acoustics, Aug. 2008.
[20] Fletcher, K., "European Conference on Spacecraft Structures, Materials and Mechanical Testing 2005" (2005).
[21] Hampton, R. D., Wiedenman, N. S. and Li, T. H., "Analytical Determination of Shock Response Spectra for an Impulse-Loaded Proportionally Damped System," Volume 1 (2004).
[22] Hampton, R. D., Nygren, K. P. and Li, T. H., "Analytical Shock Response of a Transversely Point-Loaded Linear Rectangular Plate," Volume 3: Dynamic Systems and Controls, Symposium on Design and Analysis of Advanced Structures, and Tribology (2006).
[23] Liew, K. M., Hung, K. C. and Lim, M. K., "Vibration of mindlin plates using boundary characteristic orthogonal polynomials," Journal of Sound and Vibration 182(1), 77–90 (1995).
[24] Reddy, J., "An overview of the relationships between solutions of the classical and shear deformation plate theories," Composites Science and Technology 60(12–13), 2327–2335 (2000).
[25] Reynolds, R. R., Provencher, B. D. and Shesterikov, S. A., "The high frequency, transient response of a panel with attached masses," Journal of Sound and Vibration 266(4), 833–846 (2003).
[26] Botta, F. and Cerri, G., "Shock response spectrum in plates under impulse loads," Journal of Sound and Vibration, 563–578 (2007).
[27] Parzianello, G., Francesconi, A. and Pavarin, D., "An estimation method for the Shock Response Spectrum propagating into plates subjected to hypervelocity impact," Measurement 43(1), 92–102 (2010).

[28] Lacher, A., Jüngel, N., von Wagner, U. and Bäger, A., “Analytical calculation of in-plane response of plates with concentrated masses to impact and application to pyroshock simulation,” Journal of Sound and Vibration, 3358–3370 (2012).
[29] Morais, O. and Vasques, C., “Shock environment design for space equipment testing,” Proceedings of the Institution of Mechanical Engineers, Part G: Journal of Aerospace Engineering, 1154–1167 (2017).
[30] Li, B., Li, Q., Liu, B., Niu, Z., Nangong, Z. and Zhao, C., “Critical Shock Response Spectrum of a Beam Under Shock Loading,” Volume 9: Prof. Norman Jones Honoring Symposium on Impact Engineering; Prof. Yukio Ueda Honoring Symposium on Idealized Nonlinear Mechanics for Welding and Strength of Structures (2016).
[31] Liew, K. M., “Vibration of Mindlin plates : programming the p-version Ritz Method,” Elsevier eBooks,Elsevier eBooks (1998).
[32] Lakawicz, J. M. and Bottega, W. J., “Branch dependent shear coefficients and their influence on the free vibration of Mindlin plates,” Journal of Sound and Vibration 389, 202–223 (2017).
[33] Hosseini-Hashemi, S., Zare, M. and Nazemnezhad, R., “An exact analytical approach for free vibration of Mindlin rectangular nano-plates via nonlocal elasticity,” Composite Structures 100, 290–299 (2013).
[34] Xue, K., Wang, J. F., Li, Q. H., Wang, W. Y. and Wang, P., “An Exact Series Solution for the Vibration of Mindlin Rectangular Plates with Elastically Restrained Edges,” Key Engineering Materials 572, 489–493 (2013).
[35] Srinivas, S., Joga Rao, C. V. and Rao, A. K., “An exact analysis for vibration of simply-supported homogeneous and laminated thick rectangular plates,” Journal of Sound and Vibration 12(2), 187–199 (1970).
[36] Mindlin, R. D., “Influence of Rotatory Inertia and Shear on Flexural Motions of Isotropic, Elastic Plates,” Journal of Applied Mechanics 18(1), 31–38.
[37] Bottega, W. J., “Engineering vibrations, second edition” (2014).
[38] Paz, M., “Random Vibration,” [Structural Dynamics], 479–508 (1991).
[39] Wei, JimJ. C. and Allemang, RandallJ., “Model correlation and orthogonality criteria based on reciprocal modal vectors” (1991).
[40] SATO, K. and KONDO, S., “Collapsing Behavior of Vortex Cavitation Bubble near Solid Wall under Flow Condition. Bubble Patterns from Viewpoint Perpendicular to Solid Wall.,” TRANSACTIONS OF THE JAPAN SOCIETY OF MECHANICAL ENGINEERS Series B 63(606), 372–377 (1997).
[41] Lalanne, C., “Mechanical vibrations and shock analysis, fatigue damage (iste) (volume 4)” (2014).
[42] Szuladzinski, G., “Formulas for Mechanical and Structural Shock and Impact” (2010).
[43] Hertz, Heinrich., "On the contact of solid elastic bodies and on hardness." J. Math (92), 156-171 (1881).
[44] Aidanpää, J.-O., “Review of Mechanical Vibrations by S.S. Rao” (2007).
[45] Irvine, Tom. "An introduction to the shock response spectrum." Rev P, Vibrationdata (2002).
[46] O’Hara, G. J. and Cunniff, P. F., “The shock spectrum dip effect,” Journal of Sound and Vibration 103(3), 311–321 (1985).